Unsupervised Method based on Probabilistic Neural Network for the Segmentation of Corpus Callosum in MRI Scans

Amal Jlassi[1], Khaoula ElBedoui[1,2], Walid Barhoumi[1,2] and Chokri Maktouf[3]

[1]*Université de Tunis El Manar, Institut Supérieur d'Informatique, Research Team on Intelligent Systems in Imaging and Artificial Vision (SIIVA), LR16ES06 Laboratoire de recherche en Informatique, Modélisation et Traitement de l'Information et de la Connaissance (LIMTIC), 2 Rue Bayrouni, 2080 Ariana, Tunisia*

[2]*Université de Carthage, Ecole Nationale d'Ingénieurs de Carthage, 45 Rue des Entrepreneurs, 2035 Carthage, Tunisia*

[3]*Biophysics and Nuclear Medicine Department, Pasteur Institute of Tunis, 13 Place Pasteur, 1002 Tunis, Tunisia*

Keywords: Corpus Callosum, MRI, Unsupervised Classification, Probabilistic Neural Network, Cluster Validity Index.

Abstract: In this paper, we introduce an unsupervised method for the segmentation of the Corpus Callosum (CC) from Magnetic Resonance Imaging (MRI) scans. In fact, in order to extract the CC from sagittal scans in brain MRI, we adopted the Probabilistic Neural Network (PNN) as a clustering technique. Then, we used k-means to obtain the target classes. After that, we introduced a cluster validity measure based on the maximum entropy principle (Vmep), which aims to define dynamically the optimal number of classes. The later criterion was applied in the hidden layer output of the PNN, while varying the number of classes. Finally, we isolated the CC using a spatial-based process. We validated the performance of the proposed method on two challenging datasets using objective metrics (accuracy, sensitivity, Dice coefficient, specificity and Jaccard similarity), and the obtained results proved the superiority of this method against relevant methods from the state of the art.

1 INTRODUCTION

Advances in imaging techniques during the past decade, especially in modalities of magnetic resonance, made it easy for neuroscientists and clinicians to study the Corpus Callosum (CC) in depth. Many of these studies focused on analyzing the correlation between the CC's dimensions and some neurological diseases. In fact, the CC is the largest white matter structure and the biggest fiber tract within the human brain that is responsible for the communication between the two cerebral hemispheres (Wong et al., 2006) (Waxman, 2003). It transmits visual, motoric, somatosensory, and auditory information from one hemisphere to another (Waxman, 2003) (Ganjavi et al., 2011). However, the CC shape might be the cause of some diseases such as epilepsy, Alzheimer and other types of psychosis. In a recent study, 42 patients with temporal lobe epilepsy and Hippocampal Sclerosis (HS) along with 30 subjects were studied with Diffusion Tensor Imaging (DTI) to evaluate the integrity of the CC (Lyra et al., 2017). Results showed that some clinical characteristics; like seizure frequency, duration and lesions; are associated with abnormalities in the CC. Furthermore, deformities in the CC shape had been observed in several neurodegenerative diseases such as childhood stuttering and smoking, which seemed to influence the CC shape (Choo et al., 2012) (Choi et al., 2010). Another study (Prigge et al., 2013) conducted on 917 individuals confirms that CC abnormalities might be the cause of autism. Indeed, some hypothesis implies that autism is caused by a defect in the CC which is probably related to the number of white fibers responsible for the communication between the two cerebral hemispheres. In any case, studies results can be used to predict future cases of these diseases (Lyra et al., 2017). Thus, the goal of magnetic resonance brain imaging in the framework of CC diagnosis is to unfold neurological patterns in the development of different diseases in order to enhance the related treatment (Lainhart et al., 2002). Nevertheless, the visual inspection of CC structures in MRI scans suffers from intra-variability and inter-variability between clinicians, even for experienced ones. In fact, the CC area in sagittal brain MRI slices is generally composed of different small regions forming a narrow, horizontally oriented shape which is generally located near the center of the brain (Fi-

Jlassi, A., ElBedoui, K., Barhoumi, W. and Maktouf, C.
Unsupervised Method based on Probabilistic Neural Network for the Segmentation of Corpus Callosum in MRI Scans.
DOI: 10.5220/0007400205450552
In *Proceedings of the 14th International Joint Conference on Computer Vision, Imaging and Computer Graphics Theory and Applications (VISIGRAPP 2019)*, pages 545-552
ISBN: 978-989-758-354-4

gure 1.a). However, in many sagittal brain MRI slices, the fornix appears in the neighborhood of the CC with a similar intensity (Figure 1.b). Hence, there has been a growing need for Computer-Aided Diagnosis (CAD) systems for automated analysis of the corpus callosum in MRI scans. Indeed, the subdivision of the CC is highly recommended for the parcellation task. This fact makes it possible to more effectively study brain shape and connectivity and thus to analyze the properties inside the structure (Park et al., 2008). Besides, the shape and location of CC play a very important role in identifying the brain from other tissues. In this context, various works have been focused on segmenting automatically the CC, given the strong impact of the segmentation quality on the overall precision of the CAD of the CC. Therefore, since the area of the CC is characterized by a high intensity, a precise segmentation of CC within brain MRI scans, without penetrating the irrelevant neighboring structures, is a challenging task in the diagnosis and treatment processes. To deal with this issue, we propose to automatically delimit the CC within MRI images. The contribution of this work is twofold. (1) As best as we know, we adopted for the first time the Probabilistic Neural Network (PNN) for the segmentation of CC (Cover et al., 2018). This comes from the promising results recorded by the Neural Networks (NN) within classification tasks. In fact, the most commonly used NN are radial function networks, and notably the PNN which proved its efficiency in many applications (Zhang, 2000). (2) Besides, the learning process of the proposed unsupervised PNN-based method is fully unsupervised, with no parameter adjusting and instantaneous training.

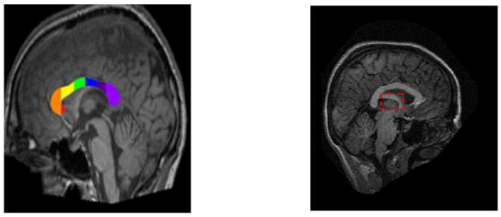

(a) (b)

Figure 1: Examples of sagittal brain MRI slices: (a) CC area is composed of rostrum (in red), genu (in orange), anterior body (in yellow), mid-body (in green), posterior body (in blue), isthmus (in purple) and splenium (in light purple). (b) An example where the fornix (framed in red) appears in the neighborhood of the CC while being of similar appearance.

The rest of this paper is organized as follows. In Section 2, we discuss the related work. Then, we describe the proposed method in Section 3. We show results in Section 4. Finally, a conclusion with some directions for future work is presented in Section 5.

2 RELATED WORK

Various 2D segmentation methods were proposed to improve the precision of the CC detection. However, the most of these methods have not overcome all challenges encountered. In fact, the CC segmentation is a challenging task given that a normal shape of the CC might not clearly highlight internal deformities, what can add complexity to the diagnosis process. Besides, many internal abnormalities might include bumps, which are hard to detect when performing CC segmentation. Existing CC segmentation methods can be regrouped into two main classes: supervised methods and unsupervised ones. On the one hand, within the class of supervised methods, a CC delineation method based on the atlas approach was developed in (Ardekani et al., 2012), where authors applied a rectangular CC search area based on a priori database information. This method consists to compute the local cross-correlation map where pixel values are represented by the cross-correlation between the warped atlas and the test image. After that, the association of a pixel to the CC region is performed by selecting the pixel having the highest cross-correlation, and a specified vote rule is applied to merge the corresponding classifications. However, this method depends on a priori information from the atlas dataset. Differently, in order to segment the CC structure, (Divya and Vishnu, 2014) proposed to start by locating coarsely the CC area. This is can be performed by the adaptive mean shift algorithm or the k-means clustering. Once the CC area is located, it is used as the initial contour for the geometric active contour. This method accuracy depends strongly on the initialization precision of the CC region, so an error initialization of the CC region can lead to an incorrect segmentation. Moreover, (Farhangi et al., 2016) proposed to embed shape information into level set image segmentation. Indeed, the CC segmentation was based on inferring shape variations by a linear combination of instances in the shape repository. This allows the guidance of segmenting curve towards the boundary of an object as well as the conservation consistent with the shapes provided in the training set. Indeed, a shift of the evolution curve at each step is done in order to minimize the Chan-Vese energy as well as towards the best approximation based on a linear combination of learning samples. This supervised method is effective only with a sufficient number of training shapes and a linear combination of learning sets. Generally, it remains true that supervised methods are conceptually simple but their robustness is strongly dependent on the accuracy of their training process. On the other hand, within the class of

unsupervised methods, a fully automated hybrid method was proposed in (Li et al., 2017). This method is based on an Adaptive Mean Shift (AMS) clustering. Indeed, to identify the CC region, an automatic CC contour initialization is performed while applying an area analysis, followed by matching template based on the shape, and locating analysis. Then, the Geometric Active Contour (GAC) model was used for the delineation of the boundaries of detected areas. Nevertheless, the application of the AMS may affect surrounding tissues to the CC cluster what causes unsatisfactory segmentation results. Thus, this method remains valid just for some specific images. In (İçer, 2013), the author presented a comparative study of Gaussian Mixture Modeling (GMM) and Fuzzy C-Means (FCM) methods for the segmentation of CC. The GMM is used to define image classes while using the weighted sum of Gaussian distributions and applying statistical decisions. By using FCM, image classes are represented by membership functions according to fuzziness information that expresses the distance from the cluster centers. Then, a maximum clustering is used to achieve the final segmentation. A fully automated method for the segmentation of CC in brain MRIs was proposed in (Tang et al., 2016). In this method, it is supported that a supervised approach can lead to a breakthrough in CC segmentation performance compared to many unsupervised segmentation methods. In order to automatically learn a set of latent features that are useful for identifying the target structures, a discriminatory learning framework was used. In the first step, a multi-atlas-based segmentation approach is used for localizing the CC structure of each image. The second step consists in the joint feature-learning and model training using a Convolutional Encoder Network (CEN). Nevertheless, this method requires a post-treatment step to reduce the amount of false positive predictions. In summary, unsupervised methods are more complex than supervised methods but they have an undeniable advantage in that they do not require prior knowledge.

3 PROPOSED METHOD

The proposed method is composed of three steps: image preprocessing using Anisotropic Diffusion Filtering (ADF), classification based on unsupervised PNN, and CC isolation using a spatial filtering.

3.1 Anisotropic Diffusion Filter

To have a good standard of the MR brain images, a preprocessing step, which allows experts or imaging modalities an efficiency of further processing, is generally required. This step aims to improve the signal-to-noise ratio, to remove undesired parts in the background, and to smooth the inner part of the region while preserving its edges. These parameters are usually influenced by other parameters such as patient comfort and physiological constraints (Demirhan et al., 2015). Therefore, we applied the ADF in order to improve the clarity of the CC within the input raw MRI scan. In fact, to deblur high-frequency noise while preserving the main edges of existing objects, the use of ADF (Perona and Malik, 1990) has proven effective. Indeed, based on its confirmed advantages, the ADF preprocessing method is frequently used in the context of MR imaging (Palma et al., 2014). The ADF uses a diffusion coefficient as an edge detector in order to obtain a smoothed image with preserved edges. In fact, to obtain the output image, we followed an iterative process based on the following equation (Kesareva, 2017):

$$I'^{(k+1)}(i,j) = \frac{I(i,j) + \lambda g(i,j) \sum_{w \in \varepsilon(i,j)} I'^{(k)}(w)}{1 + \lambda g(i,j) |\varepsilon|}, \quad (1)$$

where, I is the input image, I' is the resultant image after the k^{th} iteration, g $(= \frac{1}{1+|\nabla I|^2})$ is an edge indicator function, λ is the regularization parameter that defines the trade-off between removing noise and preserving sharp boundaries, $\varepsilon(i,j)$ denotes the neighborhood of the pixel (i,j), and $|.|$ denotes the set cardinality operator. Hence, our ADF-based preprocessing, using three iterations, allows to minimize the presence of undesired contours (Figure 2) (*e.g.* fornix contour) what optimize the overall performance of the proposed CC segmentation method.

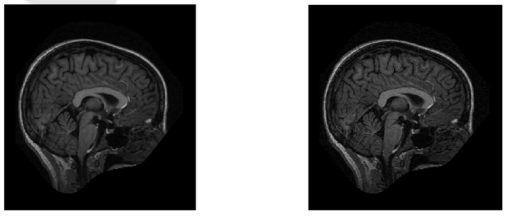

(a) (b)

Figure 2: Preprocessing using ADF: (a) Original image. (b) Filtered image.

3.2 Classification

The classification step is based on the Probabilistic Neural Network (PNN). In fact, this feed-forward neural network is used almost for classification, seen its advantage of getting better results for the Bayes-based Decision under certain conditions and its ro-

bustness against noise (Georgiadis et al., 2008). The PNN is made up of three main layers: an input layer, a hidden layer and an output layer (Shree and Kumar, 2018). In the first step, the PNN receives iteratively a D-dimensional feature vector $x = (x_1, ..., x_D)$ for the input neurons x_i $(1 \leq i \leq D)$, where D denotes the size of the input image. This vector is transmitted to the neurons in the hidden layer which is composed of nodes that are gathered in groups (each of the C classes belongs to a group). In fact, a centred Gaussian function $f(x)$ is associated with each hidden node in the class k $(1 \leq k \leq C)$, what defines the Probability Density Function (PDF) (2).

$$f_k(x) = \frac{1}{(2\pi)^{D/2}\,\sigma^D} e^{-\left(\left(\|x-x_k\|^2/(2\sigma^2)\right)\right)}, \quad (2)$$

where, σ is the smoothing parameter for the Gaussian, D is the dimension of the input vector x and $\|x-x_k\|$ is the Euclidean distance between the vector x and the centre x_k of the k^{th} cluster. At the level of the second layer, a summation of the contribution for each class of inputs is made and its total output, as a vector of probabilities, is estilatmed as follows:

$$P_k(x) = \frac{1}{(2\pi)^{D/2}\,\sigma^D C} \sum_{k=1}^{C} e^{-\left(\left(\|x-x_k\|^2/(2\sigma^2)\right)\right)}, \quad (3)$$

where C is the number of output nodes. Finally, a competitive transfer function attributes 1 for the input class that has the maximum PDF join and 0 for other classes. Therefore, Bayes decision rule under the following assumption is used to determine the class belongingness of the output x in the decision layer:

$$c(x) = \arg\max\{P_k(x)\}, \mathrm{k} = 1, 2, ..., \mathrm{C}, \quad (4)$$

where $c(x)$ is the estimated class of the output x.Accordingly, given the input image I and the interval $[C_{min} : C_{max}]$ of possible values of the number of classes in I, the unfolding stages of the proposed method, which outputs a mask M_{CC} that isolates the CC in the input image I, can be summarized as in **Algorithm 1** (such that $N = Cmax + 1 - Cmin$). In other words, the proposed classification step consists in defining the target classes (Clf_N) using k-means, then applying the PNN for the classification according to these classes. In addition, we used a cluster validity function that dynamically allows optimizing the choice of the number of classes in a given interval. In fact, for the PNN, defining the modes (centers of the Gaussian functions) is a crucial task. Then, an evaluation method, called the cluster validity, is even necessary to determine the optimal number of clusters $C*$. In order to automate the PNN, a summation of the probability density functions in the output of its hidden layer was made. It takes the form of a matrix of probabilities (PM) representing the memberships of pixels x_k to the classes C_i. This matrix will be used to calculate the Validity Index Vld by varying the class number C in a $[C_{min} : C_{max}]$ (C_{min} and C_{max} denote the minimum and the maximum number of possible classes, respectively) defined by the user. When the validity index Vld reaches its maximum value, we get the optimal number of classes that will be adopted for the classification process based also on PNN. To deal with this challenging task, the output of this PNN-based classification is a cluster map (Figure 3).

Algorithm 1: Proposed CC segmentation method.

Input: I, C_{min}, C_{max} **Output:** M_{CC}
$I' \leftarrow ADF(I)$
for $C = C_{min} : C_{max}$ **do**
  $Clf_1 ... Clf_N \leftarrow kmeans(I', C)$
end for
for $H = 1 : N$ **do**
  $PM_H \leftarrow PNN(I', Cl_H)$
end for
$Max \leftarrow 0$
for $k = 1 : N$ **do**
  if $V_{mep}(PM_k) > Max$ **then**
    $Max \leftarrow V_{mep}(PM_k)$
    $C^* \leftarrow k$
  end if
end for
$ClusterMap \leftarrow PNN(I', C^*)$
$M_{CC} \leftarrow Isolation(ClusterMap)$

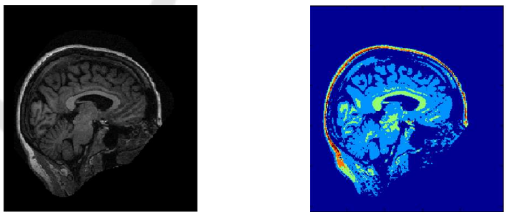

(a) (b)

Figure 3: Classification using PNN: (a) An input sagittal brain MRI. (b) Resulting cluster map generated by PNN.

In particular, we adopted the k-means method to obtain Gaussian functions centers in the hidden layer. In fact, in order to reduce the overlap of the centers, we used a spread that is equal to half of the minimum distance between the neighboring centers, in order to locally determine the widths of the radial basis functions. Indeed, the aim of clustering is to identify groups of similar pixels and thus discover an interesting distribution of model. The majority of clustering algorithms require knowledge of the right number of $C*$ classes to have an efficient classification. We are performing obliged to measure the performance of the

classification by using a validity criterion. This makes it possible to choose the optimal partition among all those obtained with the various plausible number of clusters. After a comparative study concerning cluster validity functions, we opted to use $Vmep$ index (5) which is based on the maximum entropy principle (Ammor et al., 2008) which is an automatic approach that does not require any parameter settings.

$$Vld = Vmep(PM) = \frac{1}{k}\sum_{j=1}^{k} S_j + \ln(k), \qquad (5)$$

where, $1 \leq k \leq Cl_H$ and $S_j = -\sum_{i \in Cl_H} PM_{ij} \ln(PM_{ij})$. The details of the proposed method for the automated PNN-based classification are summarized in Figure 4. Once the CC class is identified, a spatial-based filtering is applied in order to isolate the CC region. Thus, the output of the proposed method is a binary mask of the M_{CC} (0 for the background and 1 for the M_{CC}). Then, in order to define the CC contour, a follow-up algorithm applied on the border pixels of the CC region that are characterized by a maximum of the spatial gradient (Barhoumi et al., 2002).

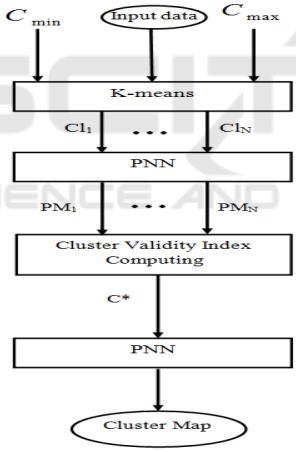

Figure 4: Outline of the proposed PNN-based classification.

4 EXPERIMENTAL RESULTS

For the evaluation of the proposed method, we used brain MRI scans from two datasets. On the one hand, we used the Open Access Series of Imaging Studies (OASIS) dataset, which is publicly available on www.oasis-brains.org. Each MR image within this dataset is composed of 128 slices with a resolution of 256×256 (1×1 mm). This dataset includes a cross-sectional collection of 416 subjects with 420 MR images, such that the majority of images are sagittal sections, for men and women aged from 18 to 96 years. The subjects are all right-handed and include individuals with early-stage Alzheimers Disease (AD). All images were acquired on a 1.5-T Vision scanner (Siemens) and using identical sequences in a single imaging session. It contains images qualified by a quality control since it excludes from the distribution of any image with severe artifacts. On the other hand, we used the MRI DICOM dataset of the head of a male professor, from the Radiology Department at the Macclesfield General Hospital, who is aged 52 years. The subject suffers from a small vertical strabismus (hypertropia), a misalignment of the eyes, which is visible in the dataset. The MRI scans within this dataset are T2 weighted turbo-spin-echo (T2W TSE) and T1 weighted Fast Field Echo (T1W FFE) with a resolution of 512×512. It is worthy noting that these datasets offer different sections (Axial section, Coronal section, and Sagittal section) what allows to study several pathologies effectively. However, clinicians usually examine the form and/or the size of the CC by visually interpreting just the sagittal sections. Thus, we used these sections to obtain accurate results on the form of CC since they allow a better analysis and diagnosis of CC-related diseases.

4.1 Qualitative Evaluation

Figure 5 shows the visual assessment of the recorded results for a sample of challenging brain MRI scans, what confirms the accuracy of the proposed method for the CC segmentation. In fact, according to our collaborator clinician expert, the CC shape and thickness are well defined and the delineated CC area shows closely the four anatomical divisions of the CC, especially the critical ones, notably the rostrum and the splenium. Furthermore, the fornix is correctly removed from the CC area. Indeed, the obtained CC masks show a precise segmentation of CC within brain MRI scans, without penetrating the irrelevant neighboring structures. Note that, within the selected sample of MRI brain scans, the CC is extracted both on female (lines 1 and 3) and male (lines 2 and 4) subjects. It is also delineated on demented (line 2) as well as non-demented subjects. Moreover, the CC extraction was performed on important (line 3) and normal intracranial volume. Moreover, Figure 6 shows an example of an incorrect segmentation, while using a relevant method for the state of the art (Li et al., 2017), of the CC. In fact, while using this method, the neighboring tissues, whose have a similar intensity to the CC, were mis-segmented as a part of the CC. However, the proposed method has successfully solved this problem within this MRI example, by recording accurate results that separate the connected regions from CC.

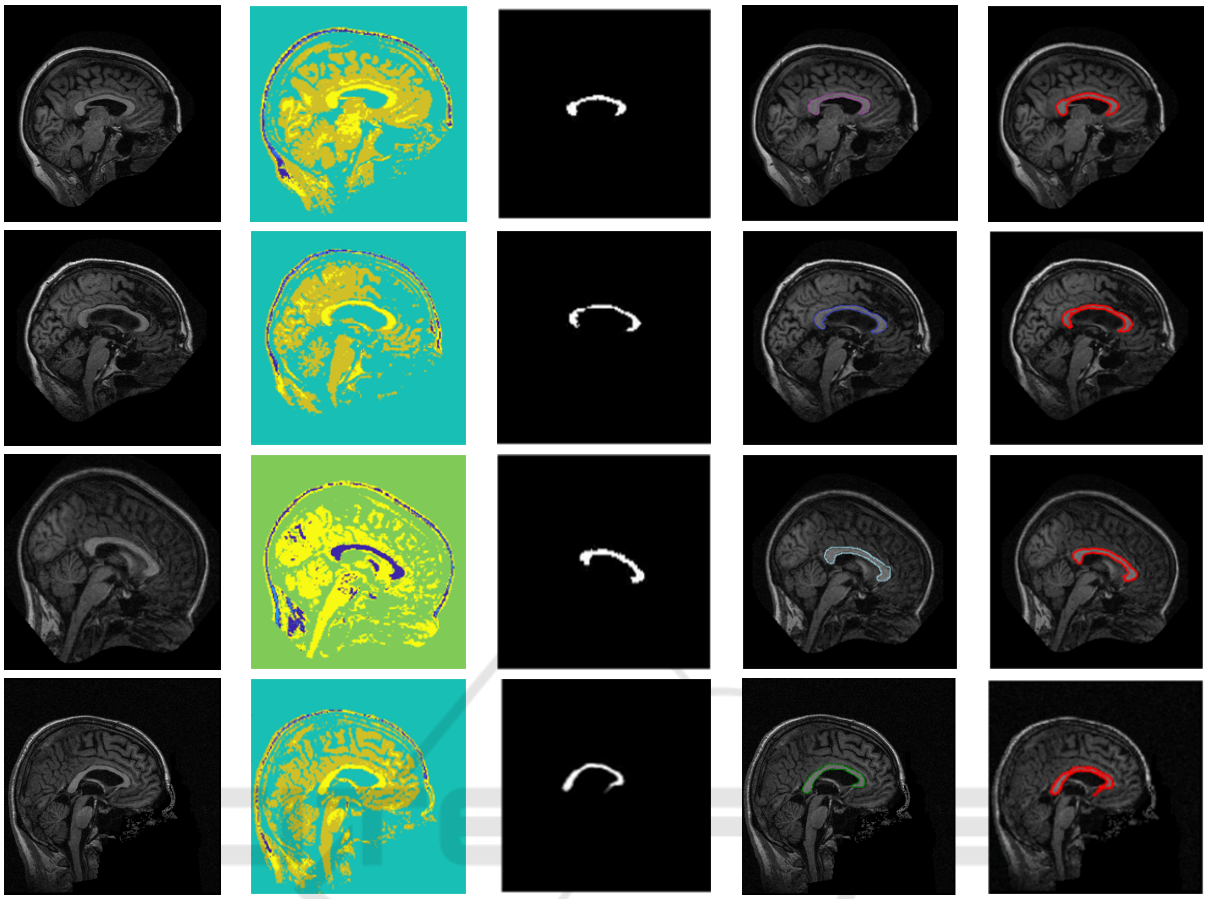

Figure 5: Qualitative evaluation: (a) Input image. (b) Cluster Map. (c) Isolated CC. (d) Ground-truth (e) Delineation of the CC bythe proposed method (except the two last MRI scans, where $C*$ is equal to 4, $C*$ is equal to 5 for the remaining scans).

Concerning the parameter tuning, it is important to notice that we set C_{min} and C_{max} to 2 and 8, respectively. This choice was motivated by the fact that this range is essential for good clustering performance as well as for the minimization of the execution time, since the MRI brain scans generally contains between 4 and 6 anatomical classes.

4.2 Quantitative Evaluation

For the quantitative evaluation of the proposed method comparatively to other relevant methods from the state of the art, we used, as evaluation metrics, the accuracy, the sensitivity, the Dice coefficient, the specificity and the Jaccard similarity. The expressions of these standard metrics are defined in Table 1, where TP refers to the True Positive (image region correctly classified as CC), TN refers to the True Negative (image region which is correctly classified as background), FP refers to the False Positive (image region which is incorrectly classified as CC) and finally FN refers to the False Negative (image region which is incorrectly classified as background). We notice that we produced, for the first time, a very useful ground-truth for CC segmentation within the challenging widely used OASIS dataset. In fact, a profes-

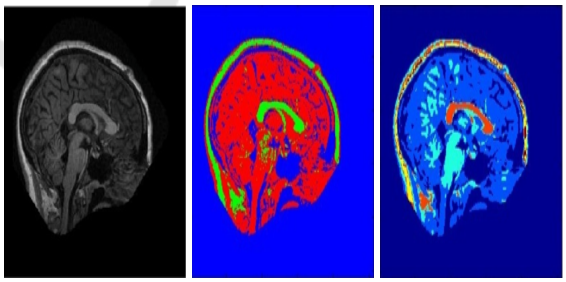

(a) (b) (c)

Figure 6: Comparison of the proposed method against a relevant AMS-based method (Li et al., 2017): (a) Input scan from the OASIS dataset. (b) Incorrect classification (fornix is classified as a part of the CC) using the AMS-based method. (c) Accurate classification using the proposed method (the maximum validity index for this scan was equal to 0.951, which corresponds to $C*$ equals to 5).

Table 1: Evaluation metrics.

Metrics	Expression	Description
Accuracy	$\frac{(TP+TN)}{(TP+FN+TN+FP)}$	It is presented as the rate of correctly classified items.
Sensitivity	$\frac{TP}{(TP+FN)}$	It refers to the proportion of positive items correctly classified.
Dice coefficient	$\frac{2\times TP}{2\times TP+FN+FP}$	It is defined as a statistical measure that is used for comparing the similarity of two sample sets.
Specificity	$\frac{TN}{(TN+FP)}$	It is the rate of negative items rightly identified.
Jaccard Similarity	$\frac{TP}{TP+FN+FP}$	It measures similarity between two sample sets.

Table 2: Evaluation of the proposed method comparatively to the other segmentation methods (Best value are on bold).

	Accuracy	Jaccard Similarity	Sensitivity	Specificity	Dice coefficient
(Li et al., 2017)	0.95 ± 0.09	–	0.84 ± 0.08	–	–
(İçer, 2013)	0.983 ± 0.0072	0.966 ± 0.0083	**0.966**	0.97	–
(İçer, 2013)	0.97 ± 0.008	0.942 ± 0.0092	**0.986**	0.934	–
(Tang et al., 2016)	–	–	–	–	0.91 ± 0.02
(Farhangi et al., 2016)	–	–	–	–	0.93
Proposed method	$\mathbf{0.99 \pm 0.005}$	$\mathbf{0.99 \pm 0.004}$	0.94 ± 0.149	$\mathbf{0.98 \pm 0.13}$	$\mathbf{0.99 \pm 0.008}$

sional neurologist from Pasteur Institute of Tunis has been charged with manually drawing the CC regions from all images belonging to the OASIS dataset. Besides, we applied a post-processing in order to exclusively extract the CC area. Table 2 shows the recorded results, where we produce the obtained performances by presenting the mean value and the standard deviation of the used objective metric. In fact, we produced the recorded metric for the proposed method as well as for five relevant CC segmentation methods from the state of the art. The compared methods are: '$AMS-ACI-GAC$' (Li et al., 2017); which combines Adaptive Mean Shift technique (AMS), Automated Initialization of CC Contour (ACI) and Geometric Active Contour model (GAC); Gaussian Mixture Model (GMM) (İçer, 2013), Fuzzy C-Means (FCM) (İçer, 2013), 'ISP into AC' that is based on Incorporating Shape Prior (ISP) into Active Contours (AC) with a Sparse Linear Combination of Training Shapes (Tang et al., 2016), '$RT-JSFE$' that uses Robust Target-Localization (RTL) and Joint Supervised Feature Extraction and Prediction (JSFE) (Farhangi et al., 2016). It is clear that the proposed method records the best Jaccard similarity score ($= 0.99 \pm 0.004$) comparatively to the compared methods. We can conclude that the proposed method localizes precisely and delimits robustly the CC (average of approximately 0.99 with 0.004 as standard deviation). This low standard deviation reflects a low dispersion of the analyzed values what it increases considerably the accuracy rate of the proposed method. Evenly, it reaches the best Dice coefficient, accuracy and specificity scores with 0.99 ± 0.008, 0.99 ± 0.005 and 0.98 ± 0.13, respectively. On the other hand, for sensitivity metric, the proposed method reaches good score and still better than $AMS-ACI-GAC$ method. The decline of the proposed method performance according to this metric can be explained by the cause of the ground-truth which is manually drawing.

5 CONCLUSION

CC is the largest white matter structure and the biggest fiber tract within the human mind that it is responsible for the communication between the two cerebral hemispheres. The CC shape might be the cause of some diseases such as autism, epilepsy and Alzheimer. Thus, the segmentation of the CC from MRI images can be used to predict future cases of diseases or to unfold neurological patterns in the development of different diseases. To deal with these challenges, we introduced an unsupervised segmentation method, which is based on the automation of the PNN. This method has been extensively validated on two challenging standard datasets. Indeed, the proposed method achieved higher performance values than relevant methods from the state of the art. Indeed, with the suggested method, the Dice coecient reached 99%, whereas specicity reached 98% and sensitivity reached 94%. Furthermore, the proposed method can be used to study the CC morphometry which is important in the diagnosis of many neurological diseases.

REFERENCES

Ammor, O., Lachkar, A., Slaoui, K., and Rais, N. (2008). Optimal fuzzy clustering in overlapping clusters. *International Arab Journal of Information Technology (IAJIT)*, 5(4).

Ardekani, B. A., Toshikazu, I., Bachman, A., and Szeszko, P. R. (2012). Multi-atlas corpus callosum segmentation with adaptive atlas selection.

Barhoumi, W., Zagrouba, E., Damiani, E., Howlett, R., and Jain, L. (2002). Boundaries detection based on polygonal approximation by genetic algorithms. *Frontiers in Artificial Intelligence and Applications. New York: Springer*, pages 1529–33.

Choi, M.-H., Lee, S.-J., Yang, J.-W., Kim, J.-H., Choi, J.-S., Park, J.-Y., Jun, J.-H., Tack, G.-R., Lee, B.-Y., Kim, H.-J., et al. (2010). Difference between smokers and non-smokers in the corpus callosum volume. *Neuroscience letters*, 485(1):71–73.

Choo, A. L., Chang, S.-E., Zengin-Bolatkale, H., Ambrose, N. G., and Loucks, T. M. (2012). Corpus callosum morphology in children who stutter. *Journal of communication disorders*, 45(4):279–289.

Cover, G., Herrera, W., Bento, M. P., Appenzeller, S., and Rittner, L. (2018). Computational methods for corpus callosum segmentation on mri: A systematic literature review. *Computer methods and programs in biomedicine*, 154:25–35.

Demirhan, A., Törü, M., and Güler, I. (2015). Segmentation of tumor and edema along with healthy tissues of brain using wavelets and neural networks. *IEEE journal of biomedical and health informatics*, 19(4):1451–1458.

Divya, Manasa, M. and Vishnu, Priya, T. (2014). A hybrid technique for the automated segmentation of corpus callosum in midsagittal brain mri. *Journal of Engineering Research and Applications*, 4(8):1–4.

Farhangi, M. M., Frigui, H., Bert, R., and Amini, A. A. (2016). Incorporating shape prior into active contours with a sparse linear combination of training shapes: Application to corpus callosum segmentation. pages 6449–6452.

Ganjavi, H., Lewis, J. D., Bellec, P., MacDonald, P. A., Waber, D. P., Evans, A. C., Karama, S., Group, B. D. C., et al. (2011). Negative associations between corpus callosum midsagittal area and iq in a representative sample of healthy children and adolescents. *PLoS One*, 6(5):e19698.

Georgiadis, P., Cavouras, D., Kalatzis, I., Daskalakis, A., Kagadis, G. C., Sifaki, K., Malamas, M., Nikiforidis, G., and Solomou, E. (2008). Improving brain tumor characterization on mri by probabilistic neural networks and non-linear transformation of textural features. *Computer methods and programs in biomedicine*, 89(1):24–32.

İçer, S. (2013). Automatic segmentation of corpus collasum using gaussian mixture modeling and fuzzy c means methods. *Computer methods and programs in biomedicine*, 112(1):38–46.

Kesareva, E. (2017). An algorithm for estimation an anisotropic diffusion filter parameter. pages 682–685.

Lainhart, J. E., Ozonoff, S., Coon, H., Krasny, L., Dinh, E., Nice, J., and McMahon, W. (2002). Autism, regression, and the broader autism phenotype. *American Journal of Medical Genetics*, 113(3):231–237.

Li, Y., Wang, H., Ahmed, N., and Mandal, M. (2017). Automated segmentation of corpus callosum in midsagittal brain mris. *ICTACT JOURNAL ON IMAGE AND VIDEO PROCESSING*, 8(1):1554–1565.

Lyra, K. P., Chaim, K. T., Leite, C. C., Park, E. J., Andrade, C. S., Passarelli, V., Valério, R. M., Jorge, C. L., Castro, L. H., and Otaduy, M. C. (2017). Corpus callosum diffusion abnormalities in refractory epilepsy associated with hippocampal sclerosis. *Epilepsy research*, 137:112–118.

Palma, C. A., Cappabianco, F. A., Ide, J. S., and Miranda, P. A. (2014). Anisotropic diffusion filtering operation and limitations-magnetic resonance imaging evaluation. *IFAC Proceedings Volumes*, 47(3):3887–3892.

Park, H.-J., Kim, J. J., Lee, S.-K., Seok, J. H., Chun, J., Kim, D. I., and Lee, J. D. (2008). Corpus callosal connection mapping using cortical gray matter parcellation and dt-mri. *Human brain mapping*, 29(5):503–516.

Perona, P. and Malik, J. (1990). Scale-space and edge detection using anisotropic diffusion. *IEEE Transactions on pattern analysis and machine intelligence*, 12(7):629–639.

Prigge, M. B., Lange, N., Bigler, E. D., Merkley, T. L., Neeley, E. S., Abildskov, T. J., Froehlich, A. L., Nielsen, J. A., Cooperrider, J. R., Cariello, A. N., et al. (2013). Corpus callosum area in children and adults with autism. *Research in autism spectrum disorders*, 7(2):221–234.

Shree, N. V. and Kumar, T. (2018). Identification and classification of brain tumor mri images with feature extraction using dwt and probabilistic neural network. *Brain informatics*, 5(1):23–30.

Tang, L. Y., Brosch, T., Liu, X., Yoo, Y., Traboulsee, A., Li, D., and Tam, R. (2016). Corpus callosum segmentation in brain mris via robust target-localization and joint supervised feature extraction and prediction. pages 406–414.

Waxman, S. (2003). *Lange clinical neuroanatomy*. New York: McGraw-Hill, 27nd edition.

Wong, T.-T., Kwan, S.-Y., Chang, K.-P., Hsiu-Mei, W., Yang, T.-F., Chen, Y.-S., and Yi-Yen, L. (2006). Corpus callosotomy in children. *Child's Nervous System*, 22(8):999–1011.

Zhang, G. P. (2000). Neural networks for classification: a survey. *IEEE Transactions on Systems, Man, and Cybernetics, Part C (Applications and Reviews)*, 30(4):451–462.